Journal of Atomic and Molecular Sciences

ISSN 2075-1303

Global Science Press

Laser Induced Dissociation Control of H_2^+ and H_3^{2+}

Z M Jia and Z N Zeng

Received: April 25, 2017,
Accepted: June 19, 2017,

DOI: 10.4208/jams.042517.061917a

http://www.global-sci.org/jams/

Abstract. Laser induced dissociation control of the symmetric diatomic molecular ion H_2^+ and the triatomic molecular ion H_3^{2+} is discussed. The simulation results demonstrate that a long-wavelength terahertz or mid-infrared laser pulse can be used to control the electrons of the dissociative states after the excitation of an ultrashort ultraviolet (UV) laser pulse. For H_2^+, there exists an effective time, which increases with increasing pulse duration of the UV laser pulse, for controlling the molecular dissociation. For the electrons of the $1s\sigma_g$ state, they move along the polarization direction of the dissociation control electric field. In contrast, for the electrons of the $2p\sigma_u$ state, they move in the opposite direction to that of the electric force. And for the triatomic molecule H_3^{2+}, the electron dissociation control can also be realized by changing the central wavelength of the exciting UV pulse.

1. Introduction

Coherent control of electrons and fragments in chemical reactions and photoelectron processes has attracted a great deal of interest. One of the main goals has been to find a way to selectively break and form molecular bonds in photochemical reactions [1–3]. As for searching the underlying mechanism in realizing electron localization control during the dissociation process, several solution routes have been proposed, including the mixture of the $1s\sigma_g$ and $2p\sigma_u$ states [4], the interference between the $2p\sigma_u$ and $3s\sigma_g$ states [5], and the superposition of the $2p\pi_g$ and $2p\pi_u$ states [6], and so on. In addition, the other quantum coupled equations [7–9] or laser-induced Stark shift effect [10–12] have also ever been used to reveal the dissociation control mechanism.

A number of theoretical and experimental studies on laser-molecule interactions have been conducted and focused on the molecular ion H_2^+, which is the simplest system having general properties of molecules. Theoretical studies have clarified that there are several dissociation mechanisms of H_2^+, such as bond softening, resonant excitation, and Coulomb explosion [13–16]. These mechanisms have been experimentally observed by utilizing pulsed lasers [17,18].

When the interaction laser pulse is very short, several new phenomenons may be found, such as the enhanced high order harmonic generation, and the generation of a single attosecond pulse [19–21]. When an ultrashort ultraviolet (UV) laser pulse, with228nm center wavelength, is used to excite the electron of the initial ground $1s\sigma_g$ state onto the first dissociaitve $2p\sigma_u$ state of the molecular ion H2+, through a one-photon process. The simulation results show that the dissociation ratio taken with 0.754fs laser pulse (the duration of the 228nm laser pulse, 1 optical cycle) can be about up to 6.9 times higher than for 3.02 fs laser pulse (4 optical cycles), due to the electron capture of the high vibrational bound states. The effective dissociation control time window of H_2^+ is increasing with the increasing pulse duration of the exciting laser pulse. Compared with the results obtained with a 7.9fs 228nm laser pulse as we adopted in our previous work [22], both the total dissociation probability and the dissociation control ratio are improved when the exciting UV pulse is changed into a one-cycle pulse, under the dissociation of a mid-infrared (MIR) laser pulse, due to the reducing of the effective dissociation control time window.

When a terahertz (THz) laser pulse is used to steer the electron motion after H_2^+ is irradiate d by an ultrashort UV laser pulse. The numerical simulation demonstrates that the ionized electron is pulled out along the polarization direction of the electric field, in contrast, the electrons in the dissociative state move in the opposite direction to that of the electric force [23]. For the dissociation of the asymmetric molecules of H_3^+ and He H_2^+, this counter-intuitive result can also be found when the two different dissociation channels $H_3^+ + n\gamma \rightarrow H_2 + p$ and $H_3^+ + n\gamma \rightarrow H_2^+ + H$, and $HeH_2^+ + n\gamma \rightarrow He+ + p$ and $HeH_2^+ + n\gamma \rightarrow \alpha + H$, for H_3^+ and HeH_2^+ are investigated, respectively [24].

It is well known that the linear triatomic molecular in H_3^{2+} does not exist in the field-free case. However, the one-electron linear H_3^{2+} can be stabilized at high intensities and frequencies, due to high nonlinear electron-field interactions [25]. The linear molecular ion H_3^{2+} can also exist in a strong magnetic field, and the direction of the molecular axis is parallel to the direction of the magnetic field [26]. Furthermore, the collision between H^+ and H_2^+ or the dissociative ionization of H_3^+ can obtain H_3^{2+}, too [27].

Compared with the simplest double-well molecular ion H_2^+ and its isotopes, the linear molecular ion H_3^{2+} includes three nuclei along the molecular axis. The simulation results show that the electron localization ratio of the middle proton is dependent on the central frequency and peak electric field amplitude of the external linearly polarized UV laser pulse. The electron localization ratio of the dissociation states of the middle proton increases from 0.3% to 50.9%, by optimizing the central frequency and peak electric field amplitude of the external UV laser pulse. Besides, a direct current (dc) electric field can be used to steer the electron motion after the excitation of an UV laser pulse. The symmetry electron localization distribution is broken seriously, as a result of the dressing effect of the dc electric field. The electrons of the dissociation states of the dressed-down potential well move opposite to the dc electric field force, and captured by the middle potential well. 68.8% electrons of all the dissociation states can be steered onto the middle proton with the variation of the amplitude of the dc electric field [28].

This paper is organized as follow: section 2 describes briefly the model systems and the parameters of the external electric fields we are using. In section 3.1, the numerical results for the exploration of the pulse duration dependence landscape of electron dynamics in

State Key Laboratory of High Field Laser Physics, Shanghai Institute of Optics and Fine Mechanics, Chinese Academy of Sciences, Shanghai 201800, China

the photodissociation of H_2^+ is studied. Section 3.2 describes the direction of the electron motion of H_2^+ in the laser induced dissociation localization. And the dissociation control of the triatomic molecule ion H_3^{2+} is discussed in section 3.3. Finally, section 4 contains a brief summary and conclusions.

Theoretical methods

We use a reduced-dimensional model for the molecular ions in the calculation. The molecular axis is assumed to be parallel to the polarization direction of the external laser fields. And the single-electron model is considered. For the symmetric linear H_3^{2+} molecular ion, the middle proton P_1 is set at the center of the coordinate system. The inter-nuclear distance of P_3 and P_2 to P_1 is R_1=R_2=R/2. That is, the external laser pulses are assumed to have no effect on the motion of the protons. Here P_2 and $P_3$are the protons locating on each side of P_1. And R is the relative inter-nuclear distance between P_2 and P_3. (And then) we can use the one-dimensional (1D) non-Born-Oppenheimer time-dependent Schrödinger equation (TDSE) to do the simulation [22–24]. The corresponding TDSE can be written as (e=$\hbar$=m_e=*1.0* in atomic unit (a.u.), which are used throughout the paper unless otherwise stated)

$$i\frac{\partial}{\partial t}\varphi(R,z;t)=[T(R,z)+V_0(R,z)+W(z,t)]\varphi(R,z;t), \quad (1)$$

where *T(R, z)* is the field-free Hamiltonian of the system. V_0(*R, z*) stands for the soft-core Coulomb interaction and *W*(*z, f*) indicates the interaction of the particle with the external laser pulses. Through this paper z represents the electronic coordinate with respect to the center of mass of the two/three nuclei, respectively. And for H_2^+, R is the relative inter-nuclear distance.

For our model, the kinetic energy in Eq. (1) reads

$$T(R,z)=-\frac{1}{m_p}\frac{\partial^2}{\partial R^2}-(\frac{2m_p+m_e}{4m_pm_e})\frac{\partial^2}{\partial z^2}, \quad (2)$$

here m_e and m_p are the electron mass and proton mass (m_p=1837), respectively.

For H_2^+, the Coulomb potential is

$$V_0(R,z)=-\frac{1}{\sqrt{(z+R/2)^2+\alpha}}-\frac{1}{\sqrt{(z-R/2)^2+\alpha}}+\frac{1}{\sqrt{R^2+\beta}}. \quad (3)$$

And for the molecular ion H_3^{2+}, the Coulomb potential can be expressed as

$$V_0(R,z)=-\frac{1}{\sqrt{(z+R/2)^2+\alpha}}-\frac{1}{\sqrt{(z-R/2)^2+\alpha}}-\frac{1}{\sqrt{z^2+\alpha}}+\frac{3}{\sqrt{R^2+\beta}}. \quad (4)$$

Where α and β are the soft-core parameters with α=1.0 and β=0.03.

W(*z,t*) is the interaction with the external laser fields, which is

$$W(z,t)=(1+\frac{m_e}{2m_p+m_e})z(E_1(t)+E_2(t-\Delta t)). \quad (5)$$

Here $E_1(t)$ and $E_2(t$-$\Delta t)$ stand for electric components of the dissociation control (THz or MIR) and UV laser fields adopted in the simulation, respectively. And Δt is the time delay between the two pulses. The total length of the two pulses is different, so Δt is defined as the difference in the on-set between the two electric fields. When the on-set of the dissociation control pulse is ahead, Δt is positive, otherwise, negative.

The time dependent electric fields of the dissociation control and UV pulses can be defined by the vector potentials $A_1(t)=-E_{10}/\omega_1\sin(\pi t/T_1)^2\cos(\omega_1 t)$ and $A_2(t)=-E_{20}/\omega_2\sin(\pi t/T_2)^2\cos(\omega_0 t+\phi)$, then the electric components of the two fields can be obtained by $E_{1/2}(t)=-\partial A_{1/2}(t)/\partial t$ [29]. Here $E_{10/20}$ is the peak intensity, $T_{1/2}$ is the duration and $\omega_{1/2}$ is the frequency of the THz (MIR)/UV pulse. And ϕ is the carrier-envelope phase (CEP) of the UV laser pulse. The total simulation time is defined by t_{end}, which can be longer than the duration of the dissociation control pulse. For time beyond, the electric field is set to be zero.

For H_2^+, the two dissociation channels are defined as

$$P_{\pm}=\int_{5.7}^{R_{\max}}dR\int_{\pm R/2.0-5.0}^{\pm R/2.0+5.0}dz\left|\varphi(z,R;t_{end})\right|^2. \quad (6)$$

Here $R_{\max}$ corresponds to the boundary of the R axis and $\varphi(z,R;t_{end})$ is the final wave function of the system. In the simulation, t_{end} is taken at 93.4 fs after the on-set of the UV pulse, when $P_{\pm}$, the probabilities of the electron being localized on one of the nuclei (left - or right +), are stable. In the calculation, we set the dissociation asymmetry parameter as $A=(P_+-P_-)/(P_++P_-)$.

For the triatomic molecular ion H_3^{2+}, the three dissociation channels, i.e., the electron localization probabilities of the left, middle and right protons are defined as

$$P_L=\int_{7.2}^{R_{\max}}dR\int_{-(R+7.3)/1.45}^{-(R-7.2)/4.0}dz\left|\varphi(R,z;t_{end})\right|^2$$

$$P_M=\int_{7.2}^{R_{\max}}dR\int_{-(R-7.2)/4.0}^{(R-7.2)/4.0}dz\left|\varphi(R,z;t_{end})\right|^2$$

$$P_R=\int_{7.2}^{R_{\max}}dR\int_{(R-7.2)/4.0}^{(R+7.3)/1.45}dz\left|\varphi(R,z;t_{end})\right|^2. \quad (7)$$

And the electron localization ratios of the dissociation states of these three protons of H_3^{2+} can be written as $L_{L/M/R}=L_{L/M/R}/(P_L+P_M+P_R)$.

3. Results and discussion

3.1 Pulse duration dependence in the photodissociation of H_2^+

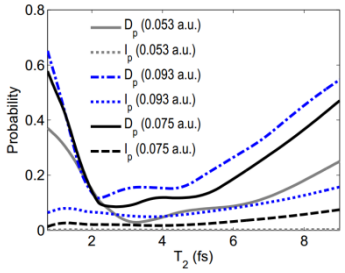

Figure 1: Dissociation and ionization probabilities, D_p and I_p, as functions of duration T_2 of the interaction 228 nm laser pulse. The peak electric field amplitudes of the UV pulse are 0.053, 0.075, and 0.093 a.u., respectively. The CEP of the pulse is 0.0.

A single short few-cycle UV pulse with a central wavelength of 228 nm is used to excite the electron wave packets of the initial ground $1s\sigma_g$ state of H_2^+ onto the first dissociative $2p\sigma_u$ state. The total dissociation ratio D_p ($D_p=\int_{5.7}^{R_{max}}dR\int_{-R/2.0-5.0}^{R/2.0+5.0}dz|\varphi(z,R;t_{end})|^2$) and the ionization probability I_p ($I_p=1.0-E_{sr}$, here $E_{sr}=\int_{0.0}^{R_{max}}dR\int_{-z_{max}}^{z_{max}}|\varphi(R,z;t_{end})|^2$ is the electron survival probability) of H_2^+ versus T_2, the duration of the interaction 228 nm laser pulse, are depicted in Figure 1. The duration of the pulse is not shorter than roughly one cycle, otherwise, the requirement $\int E_2(t)dt=0.0$ will be violated [30]. The peak electric field

amplitudes of the short few-cycle UV laser pulse are 0.053, 0.075 and 0.093 a.u., for the solid gray and black, and the dash-dot blue curves, respectively. And the CEP of the pulse is $\phi = 0.0$. From this figure, we can find that the dissociation probability is dependent on the pulse duration obviously. With increasing pulse duration, the dissociation ratio does not increase monotonously, with the same pulse intensity. Each dissociation probability curve can be split up into into three regions. In early pulse duration times, the dissociation ratio decreases with increasing pulse length, monotonously. With a continuous increase of the pulse duration, the curve oscillates. Then, the dissociation ratio shows a monotonous increase. For example, when the peak electric field amplitude of the UV pulse is E_{20}=0.075 a.u. (the corresponding intensity is 2.0×10^{14}W/cm^2), the dissociation probability curve shows a monotonous decrease during the initial region, $0.754 \leq T_2 \leq 3.02$ fs. The H_2^+ dissociation ratio taken with 0.754 fs laser pulse is about up to 6.9 times higher than for 3.02fs laser pulse. And the curve oscillates during the intermediate region, $3.02 < T_2 \leq 4.67$ fs. When T_2 is larger than 4.67fs, the curve shows a monotonous increase, see the solid balk curve of Fig. 1. When the peak electric field amplitudes of the UV pulse E_{20} are 0.053 and 0.093 a.u., the three regions in D_p can also be found, though there exist some slight differences.

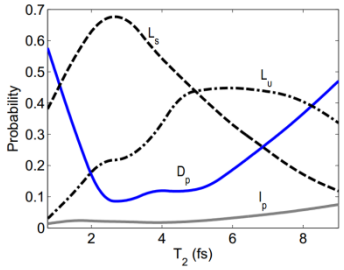

Figure 2: Electron localization probabilities of the initial and high vibrational bound states, L_s and L_v, and dissociation and ionization probabilities, D_p and I_p, as functions of duration T_2 of the 228 nm pulse. The intensity and CEP of the UV laser pulse are 2.0×10^{14} W/cm^2 and 0.0, respectively.

The participat ion of the high vibrational bound states can be used to explain the variation of the dissociation and ionization probabilities with the UV pulse duration. Figure 2 shows the electron localization probabilities of the initial and high vibrational bound states, L_s and L_v, and the dissociation and ionization probabilities, D_p and I_p, as functions of the UV pulse duration T_2. The center wavelength and intensity of the interaction laser pulse are 228 nm and 2.0×10^{14} W/cm^2, respectively. When the pulse duration is T_2=0.754 fs, 38.0% electrons are localized at the initial ground state when stable. And 57.8% electrons are excited and stabilized at the first dissociation $2p\sigma_u$ state. Only 2.89% electrons are captured by the high vibrational bound states. While with increasing pulse duration, more electrons are stabilized at the initial and intermediate states (the high vibrational bound states), and the electron dissociation probability decreases. When the pulse duration is 3.02fs, the electron localization probability of the initial ground state reaches the maximum, 67.8%. Meanwhile, the electron stabilization probability of the dissociation states reaches its minimum, 8.35%. And the electron localization probability of the intermediate states is increased from 2.89% to 21.9%. Some electrons which are excited and localized at the dissociation $2p\sigma_u$ state when the pulse duration is T_2=0.754fs are recaptured or captured by the bound states (both the initial and high vibrational bound states). It leads to the initial descending region of D_p in Fig. 1.

With a continues increase of the pulse duration T_2, the electron localization of the initial ground state decreases. Meanwhile, the electron ionization probability I_p shows a little decrease, too. For instance, when the pulse duration is T_2=3.02fs, the ionization probability is I_p=0.0197. And when T_2=4.52fs, I_p=0.0185. More electrons are captured by the intermediate states, rather than excited onto the dissociation state or ionized away. The dissociation probability curve oscillates during this section. The suppression of the ionized electrons is also caused by the electron capture of the intermediate states [20].

When the pulse duration is larger than 4.97fs, the growth of the electron localization ratio of the intermediate states slows down. And then declines with increasing T_2. Most electrons which are localized at the bound states with shorter pulse duration are excited and localized at the dissociation $2p\sigma_u$ state. Also some are ionized away. The dissociation probability D_p shows a monotonous increase during this period.

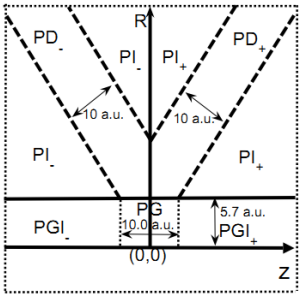

Figure 3: Schematic of the domains in configuration space defining different final states.

Figure 3 shows the different reaction channels by their position in configuration space in the photodissociation of H_2^+: $PD\pm$ for the electrons localized on the right (or left) proton, PG for the electrons of high vibrational bound states, $PGI\pm$ and $PI\pm$ for the ionized electrons defining therefore six sections. The detailed electron probabilities of these parts can be expressed as [22]

$$PG = \int_{0.0}^{5.7} dR \int_{-5.0}^{5.0} dz \left|\varphi(z,R;t)\right|^2$$

$$PGI_- = \int_{0.0}^{5.7} dR \int_{-z_{\max}}^{-5.0} dz \left|\varphi(z,R;t)\right|^2$$

$$PGI_+ = \int_{0.0}^{5.7} dR \int_{5.0}^{z_{\max}} dz \left|\varphi(z,R;t)\right|^2$$

$$PI_+ = \int_{5.7}^{R_{\max}} dR \int_{R/2.0-5.0}^{z_{\max}} dz \left|\varphi(z,R;t)\right|^2 + \int_{5.7}^{R_{\max}} dR \int_{0.0}^{R/2.0+5.0} dz \left|\varphi(z,R;t)\right|^2$$

$$PI_- = \int_{5.7}^{R_{\max}} dR \int_{-z_{\max}}^{-R/2.0-5.0} dz \left|\varphi(z,R;t)\right|^2 + \int_{5.7}^{R_{\max}} dR \int_{-R/2.0+5.0}^{0.0} dz \left|\varphi(z,R;t)\right|^2$$

$$PD_\pm = \int_{5.7}^{R_{\max}} dR \int_{\pm R/2.0-5.0}^{\pm R/2.0+5.0} dz \left|\varphi(z,R;t)\right|^2 . \quad (8)$$

A dc electric field, whose polarization is assumed to be parallel to the molecular axis, is utilized to control the electron motions of the dissociation states after the excitation of an UV laser pulse. The amplitude of the dc electric field is E_{dc}=0.008 a.u.. And for the UV laser pulse, the central frequency, intensity and CEP are 228 nm,1.0×10^{14} W/cm^2 and 0.0, respectively.

There exists an effective time, which increases with increasing nuclear mass of the molecule, for controlling the molecular dissociation [22]. The effective time for dissociation control is considered starting at the largest $|E(t)|$ of the UV laser pulse [the time t is marked as t_s], and ends at $|PG_+(t) - PG_+(t-\Delta t)|/\Delta t \cong 5.0 \times 10^{-6}$ [the time is marked as t_e], in the simulation. Here Δt is the time step. Figure 4 shows the effective time *TW* for dissociation control as a function of the duration time T_2 of the 228nm laser pulse. From this figure one can find that *TW* increases with increasing pulse duration T_2. That is because with (With) increasing T_2, the interaction time of the UV electric field on the molecule increases.

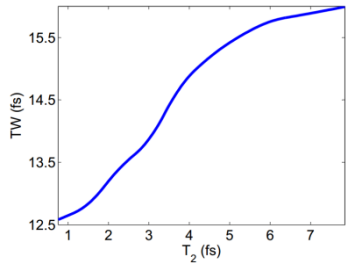

Figure 4: Effective time *TW* for dissociation control as a function of duration time T_2 of the 228 nm laser pulse. The intensity and CEP of the UV laser pulse are 1.0×10^{14} W/cm^2 and 0.0, respectively.

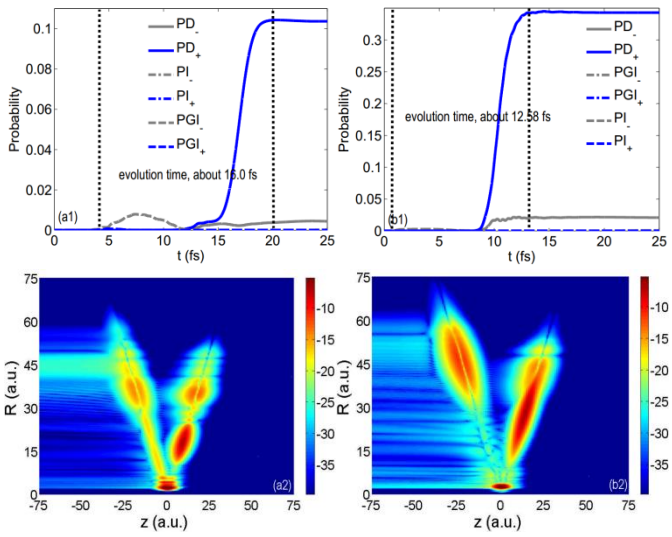

Figure 5: Upper panels: Time-dependent electron probabilities of $PD_{\pm}$, $PI_{\pm}$, and $PGI_{\pm}$ as functions of evolution time *t*. Lower panels: snapshots of the common logarithm of the electron-nuclear probability density distribution taken at t_{end}. The intensity and CEP of the 228 nm laser pulse are 1.0×10^{14} W/cm^2 and 0.0, respectively. And the amplitude of the dissociation control DC electric field is E_{dc}=0.008a.u.. The duration of the UV laser pulse is 7.9 fs for (a1) and (a2), and 0.754fs for (b1) and (b2), respectively.

When the duration of the interaction UV laser pulse is 7.9fs, the dissociation process starts at t_s=3.95fs, and ends at t_e=19.95fs. The effective dissociation control time lasts about 16.0fs, see Figure 5(a1) [22]. 1.09% electrons are ionized away along the dc electric field. While most electrons in the dissociation states, which are localized at the left proton subjected to a single UV laser pulse, are stabilized at the right proton. The total dissociation probability is 10.4%. And 96.2% electrons of all the dissociation events are localized at the right proton at the end of the simulation, as shown in Figure 5(a2).

When the pulse duration is 0.754fs, the dissociation process starts at t_s=0.38fs, and ends at t_e=12.95fs. The effective dissociation control time is changed into 12.58fs, can be seen from Figure 5(b1). The total dissociation probability is increased into 36.3%, and more than 94.7% electrons of the dissociation states are steered onto the left proton, as shown in Figure 5(b2). The total ionization probability is 0.47%.

While it is hard to obtain a dc electric field with an amplitude of 0.008a.u. in the laboratory. Laser pulse with long central wavelength, for instance, a MIR or THz laser pulse can be utilized as a substitute in the dissociation control of the molecular ion H2+. The half period of the dissociation control electric field needs to match the effective time of the molecule dissociation if a high control ratio is achieved [31]. That is to say, for the UV pulse with a duration of 7.9fs, the half period of dissociation control pulse needs to last 16.0fs. And for a single-pulse, a MIR laser pulse, whose half period is not less than 12.58fs, is satisfied. And when the starting time t_s is reset as $|PG_+(t) - PG_+(t-\Delta t)|/\Delta t \cong 5.0 \times 10^{-6}$. For the 228nm UV pulse with a duration of 7.9fs, t_s=11.71fs, and the whole dissociation control window lasts 8.24fs. While for the single-cycle 228-nm UV pulse, the starting time is t_s=8.25fs, and the dissociation control window is just 4.71 fs.

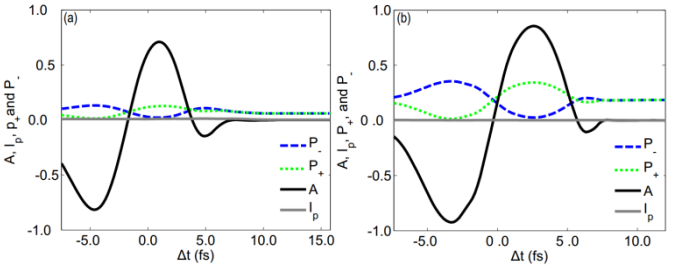

Figure 6: Asymmetry parameter *A*, total ionization probability I_p, and electron localization probabilities of the two protons $P_{\pm}$ as functions of time delay Δt. The central wavelengths and intensities of the UV and MIR laser are 228 nm, 1.0×10^{14}W/cm^2, and 3.65μm, 3.56×10^{12} W/cm^2, respectively. The pulse duration of the MIR laser pulse is 12.16 fs. And the pulse lengths of the UV pulse are 7.9fs for (a), and 0.754fs for (b).

Figure 6 depicts the two channels of H_2^+ dissociation $P_{\pm}$, the dissociation asymmetry parameter *A*, and the whole ionization probability I_p as functions of the time delay Δt between UV and MIR laser pulses. For the UV laser pulse, the central wavelength, peak intensity, and CEP are 228 nm, 1.0×10^{14}W/cm^2 and 0.0, respectively. For the MIR pulse, E_{10}=0.01 a.u. and ω_1=0.0125 a.u.. The corresponding central wavelength is 3.65 μm. And the pulse duration of the MIR laser pulse is 12.16 fs, one optical cycle.

When the pulse duration of the excitation UV laser pulse is T=7.9 fs, the largest dissociation asymmetry parameter is $|A| = 0.792$. Then the time delay of the UV and MIR laser pulses is Δt =-4.5fs, P_-=0.1326 and P_+=0.0154, 89.6% electrons of all the dissociation events are localized at the left proton at the end of the simulation, as shown in Figure 6(a). And when the pulse duration of the UV laser pulse is changed into 0.754fs, more electrons are excited onto the dissociation states. For instance, when the time delay of the two pulses is Δt =3.0fs, P_-=0.357, P_+=0.0122, the dissociation asymmetry parameter is A=-0.933,96.7%, electrons of the dissociation states are stabilized at the left proton at the end of the dissociation process, can be seen from Figure 6(b), due to the reducing of the dissociation control window.

When the molecule-laser interaction pulse is short and intense, significant CEP effects, which can be interpreted as interference between pathways requiring different numbers of photons, would be produced [32,33]. Figure 7 shows the dissociation and ionization probabilities, D_p and I_p, as functions of the CEP ϕ of the 228 nm pulse. The intensity and duration of the UV laser pulse are 1.0×10^{14}

W/cm^2 and 0.754fs (one optical cycle), respectively. I_p are multiplied by 1000 in order to show clearly. From this figure one can find that, for the total dissociation probability D_p, the CEP effects are comparatively small. Since CEP effects are the results of interference between pathways requiring different numbers of photons, the greatest modulation will be obtained when the contributing amplitudes have similar magnitude. While for the electrons of the dissociation states, the most are excited from the initial $1s\sigma_g$ state to the first dissociation $2p\sigma_u$ state through a resonant one-photon process. The resonance process leads to small CEP effects [34]. And for the ionized electrons, there does not lie a resonance process, and the CEP effects are significant, see the solid gray line in Fig. 7.

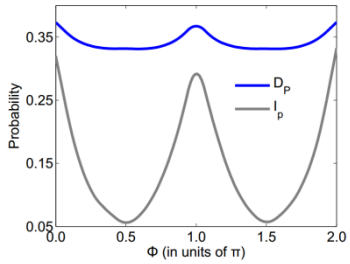

Figure 7: Dissociation and ionization probabilities, D_p and I_p, as functions of CEP ϕ of the 228 nm pulse. The intensity and duration of the UV laser pulse are 1.0×10^{14} W/cm^2 and 0.754 fs, respectively. I_p are multiplied by 1000 in order to show clearly.

3.2 The direction of the electron motion of H_2^+ in the dissociation localization

In this section, the electron movement direction of H_2^+ is studied. A THz laser pulse is used to steer the electron motion after H_2^+ is irradiated by an ultrashort UV laser pulse. In the simulation, the 228 nm UV pulse with an intensity of 2.0×10^{14} W/cm^2 and a pulse duration T_2 of 6.6fs is used to excite the electron wave packet onto the dissociative state $2p\sigma_u$. Then the 29.2μm THz pulse with an intensity of 3.0×10^{12} W/cm^2 and a pulse length T_1 of 120fs (1.23 cycle) is used to steer the electron motion. This THz pulse does not induce any further ionization and dissociation. The CEP of the UV laser pulse is ϕ =0.0 through out this section.

Figure 8 shows the dissociation asymmetry parameter A, the total ionization probability I_p, and the probabilities of the electron being localized on the left (or right) proton P_- (or P_+) as functions of, Δt the time delay between the THz and UV pulses. The intensities of these two pulses are I_1=3.0×10^{12}W/cm^2 and I_2=2.0×10^{14}W/cm^2, respectively. From Fig. 8, one (we) can find that a high degree of electron localization control in the dissociation of H_2^+ can be achieved by using the two laser pulses of UV and THz spectral regimes. There lie two time windows, $12.1\text{fs} \le \Delta t \le 41.2\text{fs}$ and $52.3\text{fs} \le \Delta t \le 80.2\,\text{fs}$, during when $|A| \ge 0.9$, more than 95% electrons of all the dissociation events can be controlled onto the left (or right) proton. For instance, when Δt=18.6fs, A=-0.982, 99.1%, electrons on the dissociation state are steered onto the left nucleus when stable, as can be seen in Figure 9(a). And when Δt=56.9 fs, A=0.978, 98.9% of all the electrons of the dissociation state localize on the right proton, as shown in Figure 9(b). For the THz pulse will also work on the molecule and a transient hetero-nuclear molecule is thus formed when the UV pulse is used to excite the electron.

The temporal evolution of the electron probabilities of different parts are presented in Figure 10. When the time delay between the UV and THz pulses is Δt=18.6fs, the dissociation process starts at t=21.9fs and ends at t=37.9 fs, for the effective dissociation control time of H_2^+ lasts 16.0fs [22]. When $19.9\text{fs} \le t \le 59.7\text{fs}$, the THz electric field is $E_1(t)<0$. The energies of the right potential well are effectively descended by $RE_1(t)/2$, while for the left well, the energies are ascended by $RE_1(t)/2$, due to the dipole interaction term $W(z,t) = (1 + m_e/(m_e + 2m_p))z(E_1(t) + E_2(t - \Delta t))$ (the electric field of the UV pulse $E_2(t - \Delta t)$ has already died off). The direction of $\overrightarrow{E_1}(t)$ is in right, and the electric field force of the electron is in the right direction for the charge on the electron is e=1.0 in the simulation. A very interesting result appears in front of us: at the end of the simulation, most electrons of all the dissociation events are stabilized on the left proton, as shown in Fig. 9(a). For the electrons on the dissociative state $2p\sigma_u$, the movement direction is opposite to the electric field force direction. The dressing field effect can be used to explain this counter-intuitive phenomenon. When the THz electric field is $E_1(t) < 0$, the potential energies of the left and right wells are effectively shifted by $\pm RE_1(t)/2$. When the distance between the two protons is small, the electron of the dissociation state $2p\sigma_u$ oscillate between them [35]. Meanwhile, the electron interacts with the protons and its kinetic energy is converted into the kinetic energy of the proton. These two protons are forced to separate and the electron makes a transition from the excited state onto the ground state as a result of the loss of energy. Due to the dressing of the THz electric field, the corresponding potential energies of the ground states of the left and the right wells are not the same. Electrons on the dissociation state are apt to jump onto the ground state of the left well, which is dressed-up. When the location probabilities are stable, one can obtain P_-=0.1531 and P_+=0.0014, respectively. Thus 99.1% electrons of all the dissociation events are localized on the left proton.

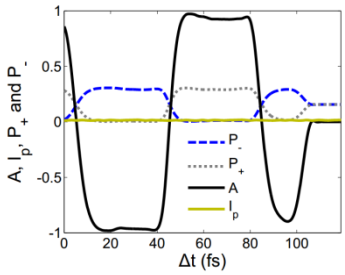

Figure 8: Dissociation asymmetry parameter A, total ionization probability I_p and $P_\pm$ as functions of Δt, time delay between the 29.2μm THz and 228nm UV pulses. The intensities of the two pulses are 3.0×10^{12} and 2.0×10^{14}W/cm^2, respectively. $P_\pm$ are multiplied by 2.0 in order to show clearly.

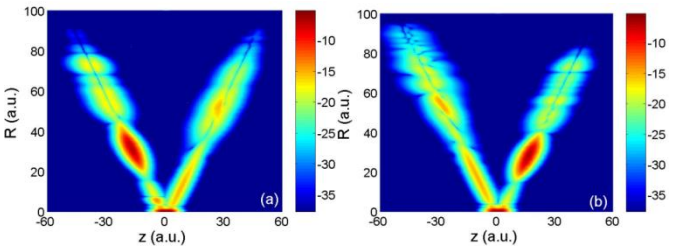

Figure 9: Snapshots of the common logarithm of the electron-nuclear probability density distribution taken at the end of the simulation. The time delay of the two pulses is Δt=18.6 fs for (a) and 56.9fs for (b).

When the time delay Δt=56.95fs, the dissociation process starts at t=60.2fs and ends at t=76.2fs, as shown in Figure 10(b). When $59.7\text{fs} \le t \le 99.5\text{fs}$, the electric field of the THz pulse is $E_1(t)$>0. The right potential well is ascended and the left one is descended. Electrons of dissociation state are apt to be captured by the right well, whose potential energies are dressed-up, though the direction of the electric field force is in left. When the dissociation

process ends, one can get P_-=0.0017 and P_+=0.1513, respectively. 98.9% of all the electrons of the dissociation events are localized on the right proton.

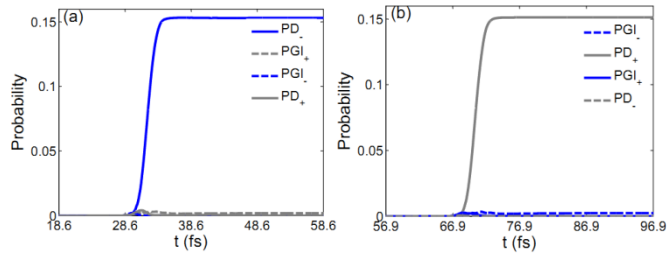

Figure 10: Time-dependent electron probabilities of $PD_{\pm}(t)$ and $PGI_{\pm}(t)$. The wavelength and intensity of the THz pulse are 29.2μm and 3.0×10^{12}W/cm^2, respectively. The time delay of the UV and THz pulses is Δt=18.6fs for (a) and 56.9fs for (b). $PI_{\pm}(t)$ near to zero and are not shown.

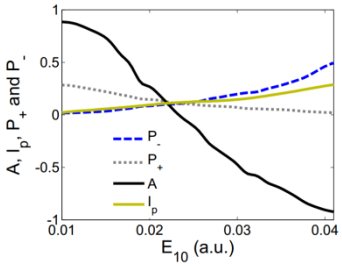

Figure 11: A, I_p and $P_{\pm}$ as functions of the electric-field strength of the THz pulse E_{10}. The intensity of the UV pulse is 2.0×10^{14} W/cm^2. The time delay between the two pulses is Δt =70.5fs. $P_{\pm}$ are multiplied by 2.0 in order to show clearly.

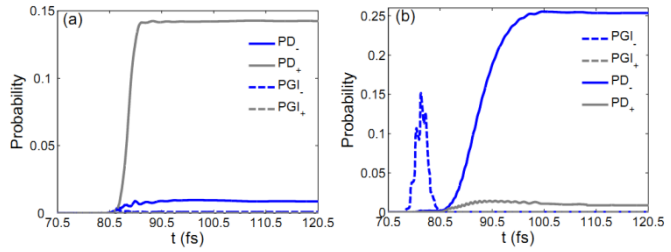

Figure 12: Time-dependent electron probabilities of $PD_{\pm}(t)$ and $PGI_{\pm}(t)$of H_2^+. The intensity of the UV pulse is 2.0×10^{14} W/cm^2 and the time delay of the two pulses is $\Delta t = 70.5$ fs. The peak intensity of the THz electric field is 0.0096a.u. for (a) and 0.0412a.u. for (b), respectively.

Figure 11 shows A, I_p, and $P_{\pm}$ as functions of E_{10}, the peak intensity of the electric field of the THz pulse. The time delay of the two pulses is Δt=70.5 fs and the intensity of the UV pulse is I_2=2.0×10^{14} W/cm^2. The localization ratio of the left proton is increasing with the increase of E_{10}. For instance, when E_{10}=0.0096a.u., P_-=0.0086 and P_+=0.1412, respectively. 5.7% electrons of all the dissociation events are localized on the left proton at the end of the simulation, as shown in Figure 12(a). And when E_{10}=0.0412a.u., P_-=0.2458 and P_+=0.0097, respectively. 96.2% of all the electrons of the dissociation state move along the electric force direction and stabilized on the left proton when stable, see Figure 12(b). Furthermore, 28.9% electrons are escaped through PGI_- for the movement direction of the ionized electrons is up to the polarization direction of the THz pulse, which is in left, as shown in Figure 13. With the increase of the intensity of the THz pulse, the motion direction of the electrons of the dissociative state is mainly dependent on the steering electric force. That is because with this increase, the ionization ratio is increased and further dissociation is induced. And more electrons are excited onto the higher $3s\sigma$ state [22]. The situation will get more complicated and further investigation needs to be done.

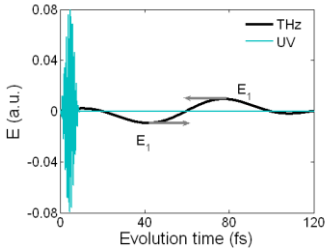

Figure 13: Electric fields of the 228nm UV and 29.2 μm THz pulses.

The electron localization of the $1s\sigma_g$ and $2p\sigma_u$ states of a double-well Coulomb potential model in an external dc electric field can be demonstrated in detail with an analytical solution. The corresponding potential curve of the Coulomb potential can be expressed as [36]

$$V(x) = C^3Sx - C^2x^2/2 + x^4/4, \quad (9)$$

where C and S are constants, and the barrier height of the double-well potential is $C^4/4$.

The trial wave packet can be written as

$$\psi(z) = a\varphi_L(z) + b\varphi_R(z), \quad (10)$$

Here $\varphi_L(z) = \varphi(z + C)$ and $\varphi_R(z) = \varphi(z - C)$ are the wave packets of the left and right potential wells, respectively. And $\varphi(z) = \sqrt{2^{1/4}\sqrt{C}/\sqrt{\pi}}\, e^{-\sqrt{2}Cx^2/2}$. The wave packets of the $1s\sigma_g$ (denoted by $|g\rangle$) and$2p\sigma_u$ ($|u\rangle$) states are

$$|g\rangle = a_1\varphi_R(z) + b_1\varphi_L(z)$$
$$|u\rangle = a_2\varphi_R(z) + b_2\varphi_L(z), \quad (11)$$

By inserting Eqs. (9) and (10) into the Schrödinger equation $H(z)\psi(z) = E\psi(z)$ and making use of $H(z) = -\partial^2/\partial z^2/2 + V(z)$, the equation can be given by

$$\begin{vmatrix} H_{LL} - \Delta H_{LR} & H_{LR} - \Delta H_{RR} \\ H_{LR} - \Delta H_{LL} & H_{RR} - \Delta H_{LR} \end{vmatrix} \begin{vmatrix} a \\ b \end{vmatrix} = E(1-\Delta^2) \begin{vmatrix} a \\ b \end{vmatrix}, \quad (12)$$

here

$$\Delta = \langle \varphi_L \| \varphi_R \rangle = \exp(-\sqrt{2}C^3)$$
$$H_{LR} = \langle \varphi_L | H | \varphi_R \rangle = \left| -C^4 + C/4/\sqrt{2} + 3/32/C^2 \right| \Delta$$
$$H_{LL} = -C^4S - C^4/4 + C/\sqrt{2} + 3/32/C^2$$
$$H_{RR} = C^4S - C^4/4 + C/\sqrt{2} + 3/32/C^2, \quad (13)$$

where Δ and H_{LR} represent the overlap integral and tunneling effect between the two potential wells, respectively. And H_{LL} and H_{RR} are the energy levels of these two well. When

$$F = C^4S$$
$$f = -C^4 + C/(4\sqrt{2}) + 3/(32C^2)$$
$$W = -C^4/4 + C/\sqrt{2} + 3/(32C^2), \quad (14)$$

one can obtain

$$H_{LR} = f\Delta$$
$$H_{RR} = W + E$$
$$H_{LL} = W - E, \quad (15)$$

here F is the external static electric field. Then we can rewrite Eq. (12) with the representation as

$$\begin{vmatrix} W - F - \Delta^2 f - E(1-\Delta^2) & \Delta f - \Delta(W+F) \\ \Delta f - \Delta(W-F) & W + F - \Delta^2 f - E(1-\Delta^2) \end{vmatrix} \begin{vmatrix} a \\ b \end{vmatrix} = 0, \quad (16)$$

the electron localization of the left and right potential wells are

$$a_1^2 = (F+\sqrt{F^2+B})^2/[A+(F+\sqrt{F^2+B})^2]$$
$$b_1^2 = A/[A+(F+\sqrt{F^2+B})^2]$$
$$a_2^2 = (F-\sqrt{F^2+B})^2/[A+(F-\sqrt{F^2+B})^2]$$
$$b_2^2 = A/[A+(F-\sqrt{F^2+B})^2], \quad (17)$$

where $A=(W-f-F)^2\Delta^2$ and $B=(W-f)^2\Delta^2$. $1-\Delta^2\approx 1$. a_1^2, a_2^2 and b_1^2, b_2^2 are the electron localization ratios of the $1s\sigma_g$ and $2p\sigma_u$ states on the left and right potential wells, respectively. The double-well potential is dependent on S. A large S will lead to a single potential well, so $S \le 4/27$ in the calculation. When $W-f \ge F$, $A = (W-f-F)^2\Delta^2 \approx (W-f)^2\Delta^2$, and $A \approx B$. The electron localization ratios of the $1s\sigma_g$ and $2p\sigma_u$ states on the right potential well can be expressed as

$$b_1^2 = B/[B+(F+\sqrt{F^2+B})^2]$$
$$b_2^2 = B/[B+(F-\sqrt{F^2+B})^2]. \quad (18)$$

When the double-well potential is definite, B is a constant. And the localization ratios are dependent on $(F+\sqrt{F^2+B})^2$ and $(F-\sqrt{F^2+B})^2$.

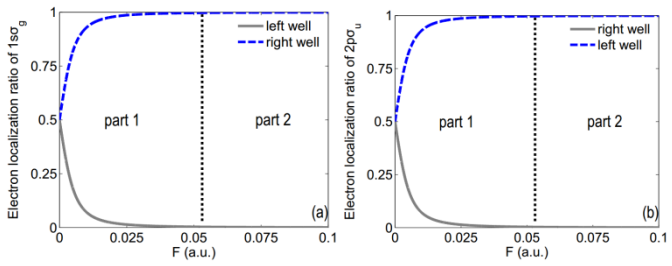

Figure 14: Electron localization ratios of the $1s\sigma_g$ and $2p\sigma_u$ states on the left and right potential wells as functions of the amplitude of the external static electric field.

When the amplitude of the external static electric field is F=0.0, $b_1^2=b_2^2=0.5$, the electron distribution of the $1s\sigma_g$ and $2p\sigma_u$ states on the left and right potential wells is symmetric. With the increasing of F, b_1^2 decreases, the electron localization ratio of the $1s\sigma_g$ state on the right potential well decreases. And for the electron localization ratio of the $2p\sigma_u$ state, with the increasing of F, $\sqrt{F^2+B}$ increases too. While F increases faster than $\sqrt{F^2+B}$ and $F \le \sqrt{F^2+B}$, $b_2^3 = B/[B+(F-\sqrt{F^2+B})^2]$ increases with the increasing of F. The electron localization ratio of the $2p\sigma_u$ state on the right potential well increases, can be seen from part 1 in Figure 14.

When $F^2 \gg B$, $\sqrt{F^2+B}$ is expanded in B/F^2, one can obtain

$$\sqrt{F^2+B} \approx F\left|1+B/(2F^2)\right|. \quad (19)$$

Then $b_1^2\approx 0.0$ and $b_2^2\approx 1.0$. For the $1s\sigma_g$ state, no electron localizes at the right potential well. And for the $2p\sigma_u$ state, all the electrons are stabilized at the right potential well, as shown in part 2 in Fig. 14. When the amplitude of the external static electric field is F<0.0, $\sqrt{F^2+B} \approx -F|1+B/(2F^2)|$. The electron localization ratios of the $1s\sigma_g$ and $2p\sigma_u$ states on the right potential well are $b_1^2 \approx 0.0$ and $b_2^2\approx 0.0$. All the electrons of the $1s\sigma_g$ state and no electron of the $2p\sigma_u$ state are localized at the right potential well.

From this section one can find that, the external dc electric field leads to a redistribution of the electrons of the $1s\sigma_g$ and $2p\sigma_u$ states of the double-well Coulomb potential model. For the electrons of the $1s\sigma_g$ state, they mainly move along the electric field force and stabilize at the dressed-down potential well. While for the electrons of the $2p\sigma_u$ state, most of which move in an opposite way as the electric field force and localize at the dressed-up potential well.

3.3 Laser-induced electron localization of linear symmetric molecular ion H_3^{2+}

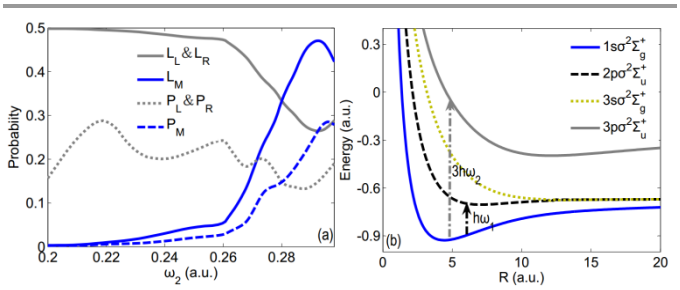

Figure 15: (a) The electron localization probabilities $P_{L/M/R}$ and localization ratios $L_{L/M/R} = P_{L/M/R}/(P_L+P_M+P_R)$ of the three protons as functions of the central frequency ω_2 of the UV laser pulse, whose intensity is 1.3×10^{14} W/cm^2. (b) The lowest four electronic energy levels of field-free linear symmetric molecular ion H_3^{2+}.

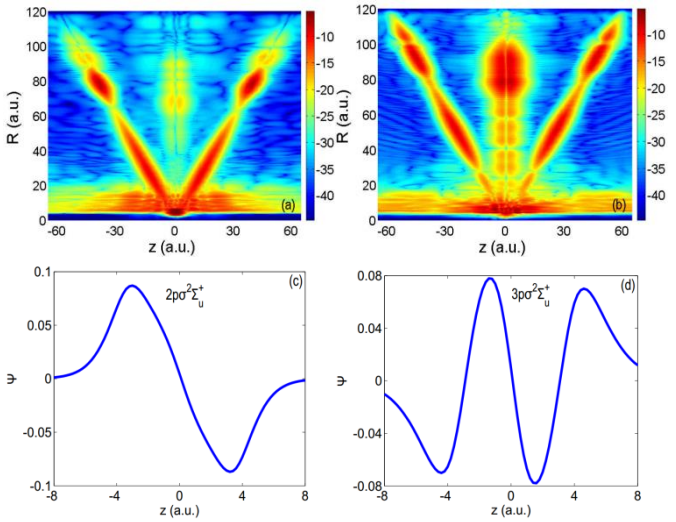

Figure 16: Upper panels: snapshots of the common logarithm of the electron-nuclear probability density distribution taken at the end of the dissociation. Lower panels: the wave functions correspond to the $2p\sigma^2\Sigma_u^+$ and $3p\sigma^2\Sigma_u^+$ states, respectively. The central frequency of the UV laser pulse is 0.2 a.u. for (a), and 0.292 a.u. for (b), respectively.

In this section, a 228nm UV pulse with an intensity of 1.3×10^{14}W/cm^2 and a pulse duration of 10.6fs is used to excite the electron wave packets of H32+ onto the dissociative states. Figure 15(a) depicts the electron localization probabilities $P_{L/M/R}$ and localization ratios $L_{L/M/R}$ of the three protons as functions of the central frequency ω_2 of the UV laser pulse. From this figure one can find that there lies a symmetric electron localization distribution with $P_L = P_R$, due to the symmetric distribution of the Coulomb potential wells of the linear molecular ion H_3^{2+}. The electron localization probabilities and localization ratios of these three protons are dependent on ω_2. When the central frequency is ω_2=0.2 a.u., the central wavelength of the UV laser pulse is 228nm. The electron localization probabilities of these three protons are $P_L = P_R = 0.1584$, and $P_M = 0.00095$, respectively. Most electrons of the dissociation states are stabilized at the protons of the two sides, as shown in Figure 16(a). When the central frequency of the UV laser pulse is 0.2a.u., about 31.8% electrons of the ground

$1s\sigma^2\Sigma_g^+$ state are excited onto the exciting $2p\sigma^2\Sigma_u^+$ state through a one-photon process, see Figure 15(b). For the electrons of the $2p\sigma^2\Sigma_u^+$ state, the most are stabilized at the protons of the two sides, and almost no electron is localized at the middle proton, due to the odd symmetry of the wave function, can be seen from Figure 16(c). At the end of the simulation, the electron localization ratios of the dissociation states of these three protons are $L_L = L_R = 0.4985$, and $L_M = 0.003$, respectively. Only 0.3% electrons of the dissociation states are localized at the middle proton.

With an increase of ω_2, more electrons of the dissociation states are captured by the middle proton. For example, when the central frequency is ω_2=0.292 a.u., the electron localization probabilities of these three protons are $P_L = P_R = 0.1458$, and $P_M = 0.2603$, respectively, can be seen from Figure 16(b). 47.2% electrons of the dissociation states are stabilized at the middle proton at the end of the simulation. When the central frequency of the UV laser pulse is ω_2=0.292a.u., some electrons of the ground state $1s\sigma^2\Sigma_g^+$ state are excited onto the higher $3p\sigma^2\Sigma_u^+$ state through a three-photon process, see Fig. 15(b). Electrons of the $3p\sigma^2\Sigma_u^+$ state can be captured by the middle proton, because the wave function includes two peaks near z=0.0a.u., as shown in Figure 16(d).

When the central frequency of the UV laser pulse is ω_2=0.292a.u., the electron localization ratio of the middle proton decreases, due to the decreasing of the electron localization probability of the $3p\sigma^2\Sigma_u^+$ state.

From Figs. 16(a) and 16(b) one can find that the electron localization starts from about $R = 7.2$ a.u.. Thus we use $R \geq 7.2$ a.u. in the definition of $P_{L/M/R}$, see Eq. (7).

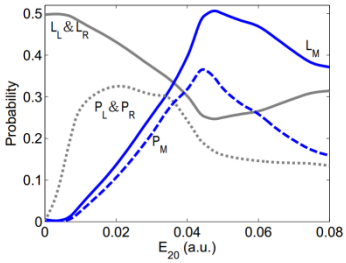

Figure 17: Electron localization probabilities $P_{L/M/R}$ and localization ratios $L_{L/M/R} = P_{L/M/R}/(P_L + P_M + P_R)$ of the three protons as functions of the the peak electric field amplitude E_{20} of the UV laser pulse. The central frequency ω_2 of the UV laser pulse is 0.292a.u..

Figure 17 depicts the electron localization probabilities $P_{L/M/R}$ and localization ratios $L_{L/M/R} = P_{L/M/R}/(P_L + P_M + P_R)$ of the three protons of the symmetric linear molecular ion H_3^{2+} as functions of the peak electric field amplitude E_{20} of the UV laser pulse. The central frequency of the UV laser pulse is 0.292a.u.. When E_{20} is low, the most electrons of the dissociation states are localized at the protons of the two sides. For instance, when the peak electric field amplitude of the UV laser pulse is E_{20}=0.007a.u., $P_L = P_R = 0.198$, and $P_M = 0.0036$, respectively. The electron localization ratios of the left and right protons are $L_L = L_R = 0.4955$, only 0.9% electrons of the dissociation states are stabilized at the middle proton. That is because when the peak intensity of the UV pulse is low, the one-photon process is dominating. The electrons of the ground state only can be excited onto the exciting $2p\sigma^2\Sigma_u^+$ state through a one-photon process. For the electrons of the $2p\sigma^2\Sigma_u^+$ state, the most are stabilized at the protons of the two sides, and almost no electron is localized at the middle proton, due to the odd symmetry of the wave function. With an increase of E_0, more electrons are localized at the middle proton. That is because when the central frequency of the UV laser pulse is 0.292a.u., the electrons of the ground state can be excited onto the higher $3p\sigma^2\Sigma_u^+$ state through a three-photon process. And the electrons of the $3p\sigma^2\Sigma_u^+$ state can be captured by the middle potential well. The excitation ratio of the three-photon process is dependent on the peak electric field amplitude E_{20} of the UV laser pulse seriously. For example, when the peak electric field amplitude is 0.0475a.u., the electron localization probabilities of these three protons are $P_L = P_R = 0.1686$, and $P_M = 0.3494$, respectively. 50.9% electrons of all the dissociation events are stabilized at the middle proton.

With a further increase of E_{20}, the electron localization probabilities of these three protons drops. More electrons are ionized and escaped away.

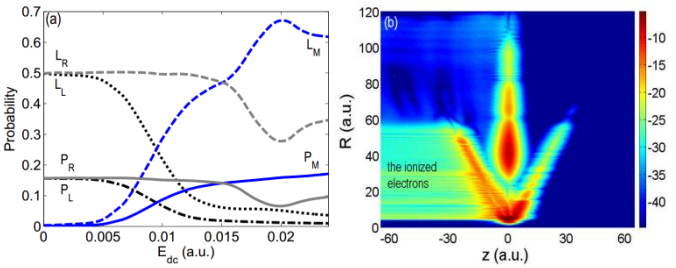

Figure 18: A dc electric is utilized to steer the electron motion of the dissociation states after the excitation of an UV laser pulse, whose central frequency and intensity are 0.2 a.u. and 1.3×10^{14} W/cm^2, respectively. (a) The electron localization probabilities $P_{L/M/R}$ and localization ratios $L_{L/M/R} = P_{L/M/R}/(P_L + P_M + P_R)$ of the three protons as functions of the amplitude E_{dc} of the dc electric field. (b) Snapshots of the common logarithm of the electron-nuclear probability density distribution taken at the end of the dissociation. The amplitude of the dc electric field is $E_{dc} = 0.02$ a.u..

The other way to enhance the electron localization ratio of the dissociation states of the middle proton is to use a dc electric field, whose polarization is assumed to be parallel to the molecular axis, to steer the electron motion after the excitation of an ultrashort UV laser pulse. For the UV pulse, the pulse duration, central laser frequency, and intensity are 10.6fs, 0.2a.u., and 1.3×10^{14}W/cm^2, respectively. Figure 18(a) shows the variation of the electron localization probabilities $P_{L/M/R}$ and the electron localization ratios $L_{L/M/R}$ of these three protons with the amplitude of the dc electric field E_{dc}. When E_{dc} nears to 0.0, there lies a symmetry electron distribution with $P_L = P_R$, and almost no electrons of the dissociation states are stabilized at the middle proton, due to symmetry distribution of the Coulomb potential wells of the linear symmetric molecular ion H32+ and the odd symmetry of the wave function of the $2p\sigma^2\Sigma_u^+$ state.

With an increase of the amplitude of the dc electric field E_{dc}, the symmetric electron localization distribution is broken seriously, as a result of the dressing effect of the dc electric field. The ionized electrons are escaped away along the dc electric field force, see Figure 18(b). While most electrons of the dissociation states, which are localized at the left proton when in a single UV laser pulse, move opposite to the dc electric field force, and are stabilized at the middle proton. The electron motion direction is the same as that of the electron of the first dissociation state $2p\sigma_u$ of H_2^+ in section 3.2. When E_{dc} >0.015a.u., the electrons on the right proton are starting to be ionized away. While the electrons of the middle proton are stabilized, due to a deeper potential well. When the amplitude of the dc electric field is E_{dc} >0.02a.u., the electron localization probabilities of these three protons are $P_L = 0.0122$, $P_M = 0.1594$, and $P_R = 0.0612$, respectively, can be seen from Fig. 18(b). 68.8% electrons of the dissociation states are stabilized at the middle

proton at the end of the simulation.

With a further increase of the amplitude of the dc electric field, the electron localization ratio of the middle proton decreases, for a further dissociation is induced.

4. Conclusions

In conclusion, the laser-induced dissociation of the symmetric diatomic molecular ion H_2^+ and the triatomic molecular ion H_3^{2+} is theoretically studied with TDSE. The dissociation probability of H_2^+ does not increase with increasing exciting pulse duration monotonously, but can be split up into three regions. The ratio decreases seriously at early pulse duration times. And then the dissociation probability curve oscillates. With a further increase of the pulse duration, the dissociation ratio shows a monotonous increase, due to the electron capture of the high vibrational bound states. The dissociation control window of the molecule ion H_2^+ is dependent on the pulse duration of the exciting pulse. The shorter pulse duration, the shorter control window. Compared with the 228nm pulse with a duration of 7.9fs, both the dissociation probability and the dissociation control ratio are improved, when the duration is changed into one optical, under the dissociation control of a min-infrared laser pulse with a central wavelength 3.65μm. Compared with a THz pulse with longer central wavelengths, a MIR laser pulse with comparable intensity is easier to obtain. Thus the proposed one-cycle 228nm laser pulse scheme enables the approach to efficiently control the electron localization during the molecular dissociation.

The electrons of the dissociative state of H_2^+ move in the opposite way as the polarization direction of the steering pulse under the influence of the dressing field effect. The analytical solution shows that the dissociation control electric field leads to a redistribution of the electrons of the $1s\sigma_g$ and $2p\sigma_u$ states. Most electrons of the $1s\sigma_g$ state are localized at the dressed-down potential well, while for the electrons of the $2p\sigma_u$ state, the most move along the opposite way to that of the electric field force and stabilize at the dressed-up potential well.

For the symmetric linear molecular ion H_3^{2+}, The numerical simulation shows that the electron localization ratio of the middle proton is dependent on the central frequency and peak electric field amplitude of the external 228nm UV laser pulse. When the electrons of the ground state are excited onto the $2p\sigma^2\Sigma_u^+$ by a one-photon process, almost no electron is stabilized at the middle proton, due to the odd symmetry of the wave function. With an increase of the central frequency of the UV laser pulse, more electrons of the dissociation states are stabilized at the middle proton, because more electrons of the ground state are excited onto the higher $3p\sigma^2\Sigma_u^+$ state through a three-photon process. The electron localization ratio of the middle proton can be raised to 50.9% by optimizing the central frequency and peak electric field amplitude of the UV pulse. Besides, a dc electric field can be utilized to control the electron motion of the dissociation states after the excitation of an ultrashort UV laser pulse. The symmetric electron localization distribution is broken seriously, due to the dressing effect of the dc electric field. The electrons of the dissociation states, which are localized at the potential well of one side, move opposite to the dc electric field force and are stabilized at the middle proton. With the changing of the amplitude of the dc electric field, 68.8% electrons of all the dissociative events can be controlled onto the middle proton.

Acknowledgements

This work was supported by the National Natural Science Foundation of China (Grant Nos. 61521093, 11134010, 11227902, and 11604349).

References

[1] B Gaire, J McKenna, M Zohrabi, K D Carnes, B D Esry and Itzhak I Ben, Phys. Rev. A, 85 (2000) 023419.
[2] V Roudnev and B D Esry, Phys. Rev. A, 76 (2007) 02340.
[3] V Roudnev V, B D Esry and Itzhak I Ben, Phys. Rev. Lett., 93 (2004) 163601.
[4] J McKenna, F Anis, A M Sayler, B Gaire, N G Johnson, E Parke, K D Carnes, B D Esry and Itzhak I Ben, Phys. Rev. A, 85 (2010) 023405.
[5] Z Wang, K L Liu , P F Lan and P X Lu, J. Phys. B, 48 (2015) 015601.
[6] F He, Phys. Rev. A, 86 (2012) 063415.
[7] M F Kling M, Ch Siedschlag, I Znakovskaya, A J Verhoef, S Zherebtsov, F Krausz, M Lezius and M J J Vrakking, Mole. Phys., 106 (2008) 455.
[8] M F Kling, Ch Siedschlag, A J Verhoef, J I Khan, M Schultze, Th Uphues, Y Ni, M Uiberacker, M Drescher, F Krausz and M J J Vrakking, Science, 312 (2006) 246.
[9] G Sansone, F Kelkensberg, Torres J F Pérez, F Morales, M F Kling, W Siu, O Ghafur, Johnsson, P M Swoboda, E Benedetti, Ferrari, F F Lépine, Vicario J L Sanz, S Zherebtsov, I Znakovskaya, A L'Huillier, M Yu Ivanov, M Nisoli, F Martín and M J J Vrakking, Nature, 465 (2010) 763.
[10] P Dietrich, M Yu Ivanov, F A Ilkov and P B Corkum, Phys. Rev. Lett., 77 (1996) 4150.
[11] H Niikura, P B Corkum and D M Villeneuve, Phys. Rev. Lett., 90 (2003) 203601.
[12] H Niikura, D M Villeneuve and P B Corkum, Phys. Rev. Lett., 92 (2004) 133002.
[13] P H Bucksbaum, A Zavriyev, H G Muller and D W Schumacher, Phys. Rev. Lett., 64 (1990) 1883.
[14] A Giusti-Suzor, X He, O Atabek and F H Mies, Phys. Rev. Lett., 64 (1990) 51501.
[15] A Giusti-Suzor and F H Mies, Phys. Rev. Lett., 68 (1992) 3869.
[16] J H Posthumus, Rep. Prog. Phys., 67 (2004) 623.
[17] K Sandig, H Figger and T W Hänsch, Phys. Rev. Lett., 85 (2000) 4876.
[18] P M Paul, E S Toma, P Breger, G Mullot, F Augé, Ph Balcou, H G Muller and P Agostini, Science, 292 (2001) 1689.
[19] J Zhou, J Peatross, M M Murnane and H C Kapteyn, Phys. Rev. Lett., 76 (1996) 752.
[20] Ivan P Christov, J Zhou, J Peatross, A Rundquist, M M Murnane and H C Kapteyn, Phys. Rev. Lett., 77 (1996) 1743.
[21] Ivan P Christov, M M Murnane and H C Kapteyn, Phys. Rev. Lett., 78 (1997) 1251.
[22] Z M Jia, Z N Zeng, R X Li, Z Z Xu and Y P Deng, Phys. Rev. A, 89 (2014) 023419.
[23] Z M Jia, Z N Zeng, R X Li and Z Z Xu, J. Phys. B, 49 (2016) 215604.
[24] Z M Jia, Z N Zeng, R X Li and Z Z Xu, J. Phys. B, 50 (2017) 035602.
[25] T Zuo and A D Bandrauk, Phys. Rev. A, 51 (1995) R26.
[26] A V Turbiner and Vieyra J C López, Phys. Rep., 424 (2006) 309.
[27] A Bandrauk, S Barmaki and G L Kamta, Phys. Rev. Lett., 98 (2007) 013001.
[28] Z M Jia, Z N Zeng and R X Li, Chin. Phys. B, 26 (2017) 013203.

Smirnova, M Spanner and M Ivanov, J. Mod. Opt., 54 (2007) 1019.
[29] D B Milošević et al, J. Phys. B, 39 (2006) R203.
[30] Z M Jia, Z N Zeng, R X Li, Z Z Xu and Y P Deng, Chin. Phys. B, 24 (2015) 013204.
[31] V Roudnev and B D Esry, Phys. Rev. Lett., 99 (2007) 220406.
[32] J J Hua and B D Esry, J. Phys. B, 42 (2009) 085601.
[33] T Nakajima and Sh Watanabe, Phys. Rev. Lett., 96 (2006) 213001.
[34] H Feng, R Camilo and B Andreas, Phys. Rev. Lett., 99 (2007) 083002.